ACS OMEGA

Open Access

http://pubs.acs.org/journal/acsodf

Article

Tuning Printability and Adhesion of a Silver-Based Ink for High-Performance Strain Gauges Manufactured via Direct Ink Writing

Md Alamgir Hossain, Gabriela Plautz-Ratkovski, Joshua DeGraff, Tarik J. Dickens, Zhiyong Liang, Curtis Hill, Jennifer Jones, and Subramanian Ramakrishnan*

Cite This: *ACS Omega* 2025, 10, 1429−1439

Read Online

ACCESS | Metrics & More | Article Recommendations | Supporting Information

ABSTRACT: Structural health monitoring (SHM) systems are critical in ensuring the safety of space exploration, as spacecraft and structures can experience detrimental stresses and strains. By deploying conventional strain gauges, SHM systems can promptly detect and assess localized strain behaviors in structures; however, these strain gauges are limited by low sensitivity (gauge factor, GF ∼ 2). This study introduces an approach to printing strain gauges with high sensitivity, while also considering stretchability and long-term durability. Through direct ink writing (DIW), these devices can be produced by the extrusion of a wide range of viscoelastic inks. The viscoelastic properties of the ink can be tuned with the help of additives to aid in the processing for a desired application. In this work, a series of inks were prepared from commercially available CB028 (silver ink used in screen printing) by adding a combination of ethyl cellulose (EC) and polyolefin (PO) (additives). With the goal of optimizing the long-term sensing response of the printed strain gauges, a systematic study of the rheological properties (frequency sweep analyses, yield stress, viscoelastic recovery, viscosity measurements, and tack tests) was conducted. A viscoelastic window approach was used to predict the optimal properties of the formulated inks. Using this approach, it was determined that 90% CB028, 5% EC, and 5% PO provided enhanced elastic properties, adhesion, and peel strength compared to commercial CB028. The formulated ink has enhanced tack (129 mN/mm^2) and peel strength (23.3 kJ/mm^2), which led to a viscoelastic window ideal for direct ink writing of the strain gauges. Printed structures were tested in a three-point bending configuration to record the piezoresistive responses that were correlated to the formulated rheological properties and underlying microstructure. The results revealed gauge factors as high as 106 with stable sensing responses for more than 300 cycles of strain. Scanning electron microscopy analysis also revealed minimal crack formation, which resulted in a stable response. The research demonstrated the feasibility of developing high-performance inks for potential printed strain gauge applications.

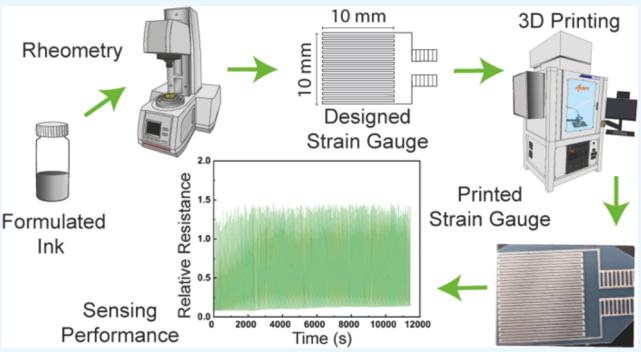

INTRODUCTION

Structural health monitoring (SHM) systems are critical to predicting the mechanical performance of equipment and structures in various industries including civil, automotive, and aerospace.[1] For example, the detection of small strains in an aircraft fuselage or space station can facilitate a better understanding and preventative maintenance of new and legacy structures. As a result, the development of SHM has drawn significant interest in the aircraft industry.[2−5] The performance of SHM is intricately linked to the manufacturing of the sensors. There are many types of sensors to consider; however, for large-scale systems, there are few that present a combination of manufacturing flexibility, low-cost, size, and shape, and enhanced sensitivity in a simple, low-profile design.[1,6,7] As a result, the metallic strain gauge has become a cornerstone in developing SHM systems.[2,6,8] Large-scale sensing systems could potentially add unwanted weight to structures (e.g., a satellite or space station), thus the development of lightweight sensors is critical; however, a major drawback to strain gauges is the relatively low sensitivity. The performance of a flexible strain gauge depends on the adhesion and cohesion of the printed silver ink. The peel performance determines the signal stability and performance durability. This is especially important for complex geometries and flexible surfaces, such as astronaut suits. Hence, there is a need to print sensors on flexible substrates with careful consideration of the adhesion/cohesion and peel properties of the printable ink. This would lead to metallic strain gauges with improved sensitivity and reliability.

Received: October 3, 2024
Revised: November 5, 2024
Accepted: November 12, 2024
Published: January 3, 2025

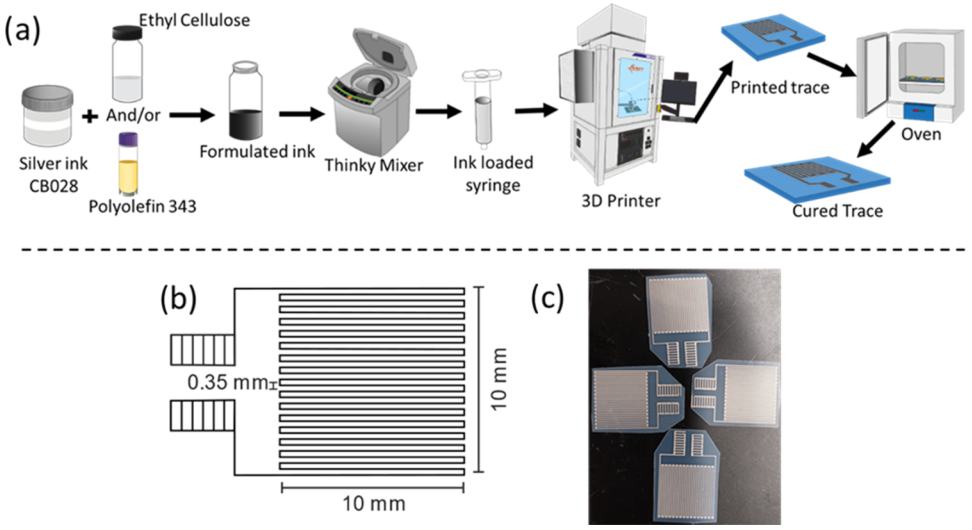

Figure 1. (a) Schematic of ink formulation, direct ink writing, and curing of the resulting sensors. (b) Schematic of strain gauge design and dimensions. (c) Picture of printed samples.

The general structure of a strain gauge consists of a flexible substrate fitted with a printed conductive metallic trace.[2,9] The electrical resistance of the trace can be measured between two terminals and monitored for piezoresistive responses to strain. The relationship between the resistance changes and the encountered strain establishes the sensing performance of the strain gauge. The translation from mechanical strain to a generated electrical signal is dictated by several factors including the piezoresistivity of the conductive trace, substrate/metal interface, tunneling effects within the particle networks, and mechanical flexibility of the trace.[8−12] Various performance parameters can be used to characterize the sensing performance of strain gauges. Sensitivity is commonly represented by the gauge factor (GF) and defined as $(\Delta R/R_0)/\varepsilon$, where ΔR, R_0, and ε denote the change in resistance, initial resistance before strain, and applied strain, respectively. In addition to the gauge factor, the performance of a strain gauge depends on its stretchability, signal stability, and durability. This research aims to develop a printable silver ink that possesses both adhesive and cohesive properties and can be used to efficiently produce strain gauges with enhanced sensitivity.

Direct ink writing (DIW) can produce miniaturized strain gauges with precision and high throughput without the need for complex tooling. This is attractive for on-demand strain gauge applications.[13,14] In addition, the shear flow generated during extrusion in DIW can assist with the dispersion of the conductive fillers throughout the ink.[15,16] This can aid in achieving high conductivity and attractive sensing performance.[15,17] DIW is compatible with inks of a wide range of viscosities (1−1,000,000 cP) and various substrate surfaces.[18]

Conductive inks typically contain conductive particles, a binder (polymer), a carrier solvent, and additives.[17] As a result, several factors need to be considered in ink selection for DIW including particle type and shape, binder material, final ink formulation, and fabrication methodology. Several particles have been explored for strain gauges, including silver flakes,[19−21] silver nanowires (NW),[22,23] carbonaceous materials like graphene,[24,25] and carbon nanotubes.[26,27] However, dispersion of carbonaceous particles in polymers is a complex and time-consuming process making ink formulation challenging.[28] Carbonaceous materials also exhibit high electrical resistivity[29] and a tendency to agglomerate that can limit processability and strain-sensing performance.[30,31]

Silver is an affordable metallic option for its good electrical conductivity and stability compared to more expensive gold and easily oxidized copper particles.[32] Due to their high aspect ratio, silver NWs are also challenging to disperse throughout a polymer matrix.[33] The piezoresistive response of NW-based sensors has also been limited due to the high contact area at NW-NW junctions.[34,35] Silver flakes are promising options for three reasons. First, they retain a large interfacial area with the polymer matrix, which helps maintain the percolation pathways during strain.[36] Second, flakes have an aspect ratio of >1, which is advantageous to achieving electrical percolation at low concentrations of silver.[37] Lastly, silver oxidizes slower than other attractive metals (e.g., Cu, Al, and Ni).[38] These reasons provide incentives for companies like DuPont, Novacentrix, and Henkel to produce a variety of silver inks.[39] However, these inks have mainly been developed for screen printing. There have been very few studies on the DIW of CB028 (DuPont) for the manufacture of strain gauges.

The viscoelasticity of polymer-based metallic ink plays a critical role in printing strain gauges. After extrusion, the adhesion between the ink and the substrate must be robust. Many inks contain polymeric binders with functional groups that promote adhesion;[40] however, enhancing the adhesion of printed traces is still a significant challenge.[41] In addition, the printed traces must exhibit elasticity and toughness to withstand repetitive mechanical stress during strain operations. Due to the high loading of silver (∼80 wt %) and low amount of binder material, silver ink has been susceptible to both weak adhesive properties and poor elasticity.[42−45] Elasticity is a prerequisite to achieving stable electrical responses under repetitive strain cycles.[34,,47]

This research will explore the tunability of silver ink, as it can be modified with polymer additives to improve adhesive (e.g., tack and peel strength) and cohesive properties (e.g., flexibility and toughness).[19] Ethyl cellulose (EC), which is compatible with a number of organic materials, has proven to be a promising polymer binder.[48,49] Since a natural polymer like EC can exhibit brittle cracking, adding a plasticizer is necessary.[50]

https://doi.org/10.1021/acsomega.4c09042
ACS Omega 2025, 10, 1429−1439

EC possesses intermolecular cohesive strength that could prevent printed traces from peeling away from the substrate; however, adding the plasticizer can enhance both adhesion and fracture toughness.

In the current work, it is our aim to demonstrate the enhanced sensing performance of printable silver inks by mixing an EC polymer binder and a polyolefin (PO) adhesion modifier that can also serve as a plasticizer. The strain-sensing performance of the printed inks was explored and correlated to the rheological properties of the formulated inks. In addition, the adhesion, cohesion, tack, and peel properties of the inks were studied by using viscoelastic frequency sweeps, tack experiments, and a viscoelastic window (VW) approach that uncovers potential design rules for ink formulation. The results establish structure-processing-performance relationships that reveal the impact of the ink formulation on the gauge factor and response stability of the manufactured strain gauges.

MATERIALS AND METHODS

Materials. A commercial silver-based ink (CB028) was purchased from DuPont. According to the manufacturer datasheet, the ink contained 60−70 wt % of silver flakes (particle size 8−10 μm), 0.1−1.0% of fatty acids amine, and 29−39% of undisclosed materials. Chlorinated polyolefin (PO) 343 purchased from Eastman was used as an adhesion modifier and plasticizer. Ethyl cellulose (EC, viscosity 10 cP - 5% in toluene/ethanol, 4:1) purchased from Ashland Chemicals was used as a binder.

Ink Formulation. Inks were formulated by following the procedure illustrated in Figure 1a. EC and/or PO were dispersed into the CB028 ink using a high-speed planetary mixer (THINKY ARE-310). For each ink preparation, EC and PO were added incrementally (0.1 g or less in each step) to ensure uniform dispersion and mixing throughout the base ink. Each mixing step involved 4 min of mixing at 2000 rpm and subsequent degassing for 2 min at 2200 rpm. Rheological experiments and sensor printing were performed with four formulations: (1) 100 wt % CB028, (2) 95 wt % CB028 and 5 wt % EC, (3) 90 wt % CB028, 5% EC and 5 wt % PO, and (4) 95 wt % CB028 and 5 wt % PO. The remaining sections will denote the four inks as CB028, 5%EC, 5%EC5%PO, and 5% PO. Formulating inks to achieve the desired printed performance requires a fine balance between the amount of conductive particles, binder, and underlying matrix. Different constituents need to be tuned to achieve the desired printability, adhesion, cohesion, tack, and peel. CB028 is the base case that needs improvement. As shown in subsequent sections, printed traces of CB028 crack under strain. 5%EC involves the addition of a cohesion modifier, which improves the elasticity of the inks. However, a higher amount of EC does not make it printable due to high viscosity and reduced wettability. 5% PO improves wettability, but higher amounts result in a brittle structure and a reduction in viscosity (poor printability). Thus, 5% EC and 5% PO, which involve both compounds, were formulated to print a sensor that has the desired characteristics. Increasing the amounts of EC and PO decreases the wt % of silver particles, which increases resistivity. 5%EC5%PO, which contains 90% CB028, has a silver loading of ∼63 wt % (CB028 has a silver loading of ∼70 wt % as mentioned in the manufacturers datasheet), which is just higher than the percolation limit of silver in the polymer matrix.[51]

Rheology. The rheological behavior of formulated inks is critical to extrusion, the ink−substrate interface, and overall strain-sensing performance. The inks should have sufficient elasticity and viscosity to be printable. The printing pressure should be higher than the yield stress of the material, so that it flows. Moreover, once printed, the elastic properties should recover over time so that the particle network recovers from high shear. Rheological properties were characterized using an MCR 302 rheometer (Anton Paar, Ashland VA) with a cone and plate geometry (25 mm diameter, 1° angle). Yield stresses were determined using an amplitude sweep (strain range of 0.005%−30%), and the point of intersection of the storage modulus (G') and loss modulus (G'') during the sweep was taken as the yield stress/strain.[16,52,53] The viscoelastic recovery tests (G' recovery) involved experiments performed in three intervals: (1) oscillation at 1 Hz and 0.005% strain in the linear viscoelastic region (LVR) was performed for 250 s, (2) a constant shear of 200 s^{-1} for 5 s was applied to simulate printing conditions,[54] and (3) oscillation at 1 Hz and 0.005% strain (LVR) was performed for 1500 s to observe the recovery of the storage modulus. Viscoelastic measurements of G' and G'' were carried out using a frequency sweep (0.1−10 Hz) at a strain of 0.005%. Lastly, for the flow curves (viscosity vs shear rate), a shear rate range of 0.1−50 s^{-1} was utilized.

A method to conduct direct tack and peel tests was also developed by using rheometry. Tack and peel tests were performed on the rheometer using a parallel plate geometry (8 mm diameter). A poly(ethylene terephthalate) (PET) substrate was attached to each plate using double-sided tape. A small quantity of ink was placed on the bottom substrate, and the top plate was lowered until it contacts the ink. To begin the test, the gap between the plates was maintained at 0.1 mm for 5 s. Then, the top plate was raised at a constant velocity of 0.05 mm/s, and the normal force was measured as a function of the separation between the plates generating a stress−distance curve. The formulated ink must exhibit tack and a balanced viscoelastic profile that promotes wettability, cohesion, and peel. Frequency sweeps as determined above provide valuable information about adhesion and cohesion at low and high frequencies, respectively. In addition, the tack tests offer valuable insight into adhesion and cohesion that influence the bonding properties of viscoelastic inks. All measurements on the rheometer were performed at a constant temperature of 25 °C.

Direct Ink Writing Process. A nScrypt 3Dn 300 printer was used to accomplish direct ink writing of silver ink traces. The printer was equipped with SmartPump and nStudio navigation software. To start the printing process, silver ink was loaded into a 3 mL Luerlock syringe (Nordson EFD, Westlake, OH). Using a syringe coupler, the syringe was mounted horizontally onto the SmartPump and orthogonally in the extrusion direction. A 55 μm gap was maintained between the nozzle tip and substrate during the printing process, and the print speed was set at 10 mm/s. The inks were extruded through a 100 μm, tapered-type ceramic precision nozzle. The extrusion pressure was varied between 8 and 34 psi. After preliminary trials, the final sensor design included thirty-two 10 mm-long traces joined at each end by 0.35 mm-long traces in a serpentine pattern, as illustrated in Figure 1b, and the printed samples are shown in Figure 1c. The dimensions were chosen after trials to achieve a certain resistance and to reduce the variability in measurements of resistance and the signal-to-noise ratio.The serpentine pattern is typical for metallic strain gauges for higher strain

https://doi.org/10.1021/acsomega.4c09042
ACS Omega 2025, 10, 1429−1439

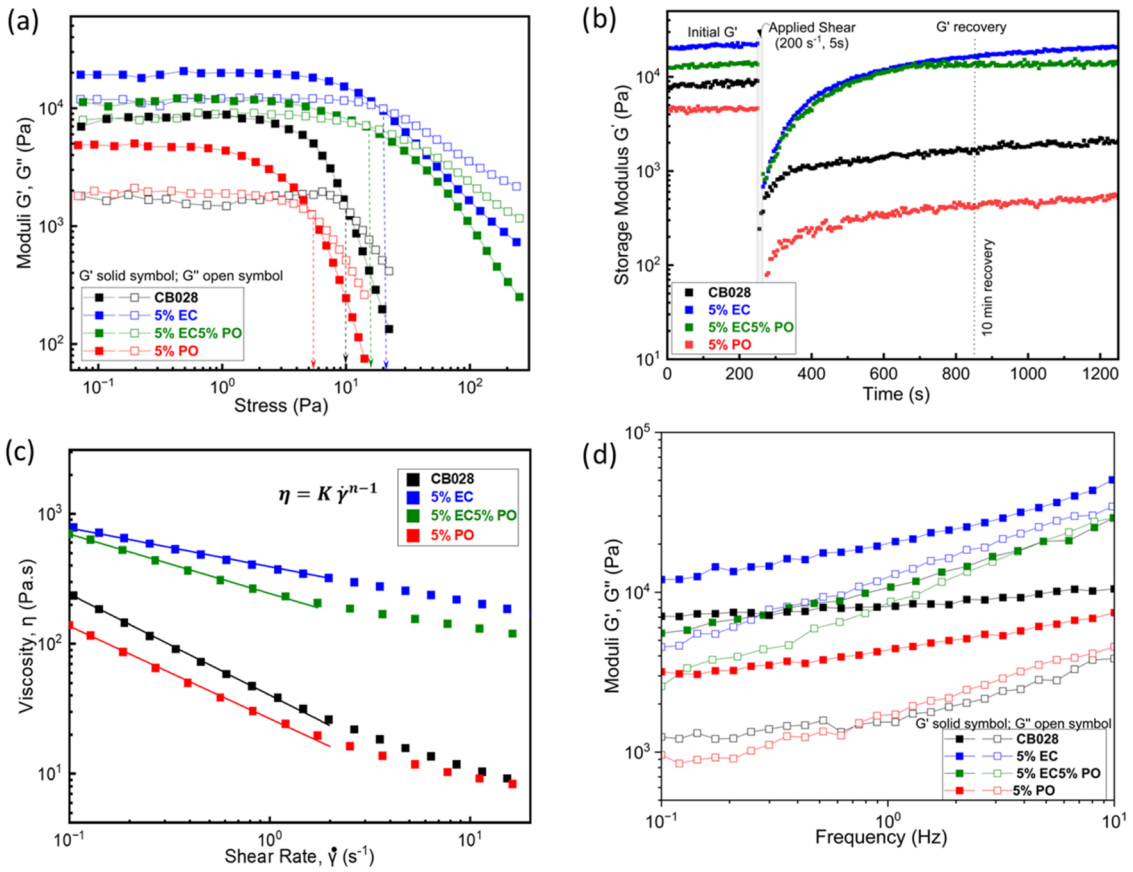

Figure 2. Rheological measurement of silver-based inks. (a) Moduli as a function of applied stress for the different formulations studied in this work. (b) Storage modulus as a function of time after applied shear (recovery test) for the different formulations. A constant shear of 200 s^{-1} is applied for 5 s after which the growth of G' with time was measured. (c) Viscosity as a function of shear rate for the different formulations. The solid square markers are the experimental measurements, while the solid lines are curves fit to the power law model. (d) G' and G'' as a function of frequency (0.1−10 Hz) for silver-based inks. The symbols are experimental data points, and the lines are drawn to guide the eye.

sensitivity.[55,56] After printing, the traces were cured in an oven at 160 °C for 1 h.

Resistivity Measurement. The electrical resistivity of the individual silver traces was directly measured at room temperature according to ASTM D257-14.[57] The electrical resistivity (ρ) can be calculated by using eq 1.

$$\rho = R\frac{A}{L} \tag{1}$$

R, A, and L denote the trace resistance, cross-sectional area, and length, respectively. R was measured using a two-probe connection and a Keithley 2400 multimeter. Images of the cross section were obtained from an optical microscope and the area calculated (Supporting Information, Figure S1).

Strain-Sensing Performance. After the traces were printed, the strain gauge was trimmed and crimped at the terminals with aluminum soldering contacts for easy wiring. The sensor was then fastened to an acrylonitrile butadiene styrene (ABS) bar with an adhesive (Loctite 401). Three-point bending experiments were performed according to the methods in ASTM D7264.[58] A Shimadzu mechanical tester was used to apply controlled strains to the ABS bar and the attached strain gauge. The length (L) and thickness (h) of the support bar were 50 and 6.25 mm, respectively. The bending strain (ε) was calculated using eq 2.

$$\varepsilon = \frac{6\delta h}{L^2} \tag{2}$$

Here, δ denotes the midspan deflection. The electrical response to strain was recorded using a multimeter and LabView software.

Scanning Electron Microscopy Imaging. The morphology of the printed traces was examined by using a field emission scanning electron microscope (FESEM; Helios G4 UC). Double-sided adhesive carbon tape was used to fasten the sensor to the sample holder and to facilitate the electrical conductivity from the trace to the holder for grounding. To improve the imaging contrast, an ∼3 nm layer of gold was sputtered on the trace's surface. During imaging, an accelerated voltage and working distance of 10 kV and ∼4.1 mm was respectively maintained.

RESULTS AND DISCUSSION

Yield Stress and Viscoelastic Recovery. A principal aim of this work is to use rheological characterization in support of developing inks to print strain sensors. A key rheological property is the yield stress, which is the minimum stress required to break the particle/polymer network and is indicative of the minimum extrusion pressure required to initiate material flow.[59] The ink must exhibit a sufficiently low yield stress to extrude continuous silver traces through a 100 μm nozzle.[53,59] As displayed in Figure 2a, the yield stress can

https://doi.org/10.1021/acsomega.4c09042
ACS Omega 2025, 10, 1429−1439

be directly measured from amplitude sweep experiments. As stress increases, the particle network breaks, resulting in a decrease in storage modulus (G'). The intersection of G' and the loss modulus (G'') can be used to determine the yield stress of the ink.[16,52] It is apparent throughout this research that the addition of EC and PO to CB028 alters the viscoelastic behaviors of the silver ink.

EC is commonly used as a cohesion modifier in composite formulation.[60] As a result, the yield stress of 5%EC (20 Pa) was nearly double that of the yield stress of pristine CB028 (10 Pa). The increase in storage modulus and yield stress can be attributed to the enhanced cohesion between silver particles due to the network forming ability of EC caused by hydrogen bonding. On the contrary, the yield stress of 5%PO (5.5 Pa) was nearly half of the yield stress of pristine CB028. PO acts as a diluent, as it contains low-molecular-weight compounds that have minimal effect on enhancing the network formation among the silver particles. This is reflected by the reduction in the moduli and yield stress of the ink formulations that contain PO.[60,61]

During extrusion, viscoelastic inks experience high shear, which breaks the particle network and reduces the storage modulus. Hence, to maintain the desired shape after extrusion, the ink must exhibit viscoelastic recovery immediately after printing. This can be signified by a rapid recovery of the storage modulus after shear strain.[16] In this study, the shear rate of extrusion through a 100 μm nozzle was calculated to be ~200 s^{-1} [54,62] Hence, a shear rate of 200 s^{-1} was applied to the formulated inks for 5 s to monitor the recovery of G' for the subsequent 15 min. Figure 2b presents the results. After 10 min, the G' recovery of CB028, 5%EC, 5%EC5%PO, and 5% PO were almost 17, 60, 100, and 9%, respectively. These results highlight the synergistic effect of adding both PO and EC into the silver ink. Since PO behaves as a diluent, the viscoelastic recovery of 5%PO is poor. Though 5%EC improves the storage modulus, the full recovery of G' requires more time than 5%EC5%PO. Thus, the combination of EC and PO could offer a pathway for optimizing the viscoelasticity profile of the CB028 ink for printing strain gauges via DIW.

Flow Curves and Shear-Thinning Behavior. In addition to viscoelasticity, it is important for the formulated inks to exhibit shear-thinning behavior, which greatly aids in the DIW printing process. Figure 2c plots the viscosity as a function of shear rate for the four different inks used in this work. The shear-thinning behavior can be quantified using the power law model expressed in eq 3.[16,59]

$$\eta = K\dot{\gamma}^{n-1} \tag{3}$$

Here, η denotes the viscosity (Pa·s); K denotes the flow consistency index (Pa·s^n) related to molecular mobility; $\dot{\gamma}$ denotes the shear rate (s^{-1}); and n denotes the flow index, which quantifies the shear-thinning behavior. Newtonian fluids exhibit a flow index close to 1, whereas non-Newtonian fluids exhibit behaviors from low shear-thinning ($n \sim 0.8$) to high shear-thinning ($n \sim 0.2$).[52] The calculated values of K and n for the different formulations are presented in Table 1. Pristine CB028 exhibits high shear-thinning behavior ($n = 0.22$). The addition of EC reduces this effect, as n approaches a value of 0.7 (for 5%EC). Though the addition of PO ($n = 0.27$) slightly increases the flow index compared to that of pristine CB028, combining it with EC produces an ink with moderate shear-thinning behavior ($n = 0.54$). The consistency index, K, is a measure of zero-shear, non-Newtonian viscosity. For CB028, 5%EC, 5%EC5%PO, and 5%PO, K was measured to be 40 Pa·s^n, 394 Pa·s^n, 244 Pa·s^n, and 26 Pa·s^n, respectively. As the high molecular EC acts as a cohesive modifier and increases viscosity, the low-molecular weight PO acts as a diluent and reduces viscosity. The difference in molecular entanglement is reflected in the difference in the K values.

Table 1. Calculated Values of K and n using the Data from Figure 2c for the Different Ink Formulations

ink	K (Pa·s)	n	R^2
CB028	40.33 ± 0.66	0.22 ± 0.00	0.999
5%EC	394.78 ± 2.76	0.70 ± 0.00	0.999
5%EC5%PO	244.21 ± 4.12	0.54 ± 0.00	0.998
5% PO	26.62 ± 0.82	0.27 ± 0.02	0.998

Frequency Response Determination. The formulated inks must possess adhesive properties that facilitate bonding at the ink/substrate interface to enhance stress transfer from the substrate into the piezoresistive silver network. This bonding and debonding behavior is influenced by viscoelastic properties. More specifically, the storage modulus response at low and high frequencies reveals the balance between adhesion and cohesion.[74] In the DIW processes, the extruded ink adheres to the substrate slowly on longer time scales, which correlate with low frequency. On the other hand, debonding, which is associated with cohesive properties like peel strength, can be described by the high-frequency response of the storage modulus.[63] The peeling of ink is abrupt and associated with a shorter time scale or a high-frequency response. Hence, the bonding and debonding behaviors of viscoelastic silver ink can be evaluated through a frequency sweep of the storage modulus within the linear viscoelastic region (LVR). The resulting data can be plotted and visualized as a viscoelastic window (VW, section 4.5). The VW of each ink can be compared to predict its bonding and debonding behaviors.

To effectively analyze the balance of adhesive and cohesive properties in viscoelastic inks, it is necessary to measure the viscoelastic properties across a 100-fold difference in frequency.[64] Therefore, the bonding and debonding behaviors were evaluated at 0.1 and 10 Hz, respectively. Tack, which can be estimated through the ratio of G' at 10 Hz to G' at 0.1 Hz, can be related to stickiness. It describes a critical combination of adhesive and cohesive forces that influence the behaviors at the ink−substrate interface. A higher ratio (higher tack) implies both high cohesion and high adhesion, as a high G' at high frequencies can be correlated to increased cohesion and peel strength, while a low G' at low frequencies can be correlated to increased wettability/adhesion.[63,65]

Figure 2d presents the G' and G'' of the four ink formulations as a function of frequency. Table 2 presents the resulting values of the storage moduli and tack. For pristine CB028, the tack ratio of 1.4 is relatively low due to a combination of moderate adhesion and poor cohesion, which is represented by the low G' at 10 Hz. The polymer additives have a profound impact on the wettability, adhesion, cohesion, and debonding of the formulated inks.[66] Addition of EC increased the ratio to 4.2. This could be attributed to the enhanced cohesive properties resulting from the strengthened structure of the silver particles and hydrogen bonding between the EC chains. As summarized in Table 2, at 0.1 Hz, 5%EC exhibited a 61% higher G' value (12.02 kPa) than that of CB028 (7.49 kPa). EC also effectively improves debonding behavior effectively. At 10 Hz, 5%EC exhibited a G' (50.5 kPa)

https://doi.org/10.1021/acsomega.4c09042
ACS Omega 2025, 10, 1429−1439

Table 2. Storage Modulus (G') at 0.1 and 10 Hz for the Different Ink Formulations

	G' (Pa)			
inks	0.1 Hz	10 Hz	G'(10 Hz)/G'(0.1 Hz) tack	comments[65,67]
CB028	7488	10,500	1.40	moderate adhesion, poor cohesion, low tack
5%EC	12,016	50,504	4.20	lowest adhesion, highest cohesion, moderate tack
5%EC5%PO	5552	29,130	5.25	higher adhesion, higher cohesion, high tack
5%PO	3182	7458	2.34	higher adhesion, poor cohesion, low tack

nearly five times higher than CB028 (10.5 kPa). Although the loss modulus (G'') can also be used similar prediction, the values are less pronounced.[65]

Lower molecular weight plasticizers can act as diluents that promote both reduced viscosity and storage modulus.[64] For example, the addition of PO reduces G' at 0.1 Hz promoting improved wettability; however, it also reduces the high-frequency G' response, which is associated with cohesion. Though the tack ratio (2.34) is higher than that of pristine CB028, it is nearly half of the ratio for 5%EC. As seen in Table 2, at 0.1 Hz, 5%PO shows a 58% lower G' value (3.18 kPa) compared to CB028. This result indicates that PO enhances wettability for improved adhesion; however, PO also reduces the high-frequency G' value by 42% compared to CB028, implying that it exhibits poorer cohesive properties and debonding characteristics. Combining EC and PO produces a ratio that encompasses both lowered G' at 0.1 Hz and high G' at 10 Hz, giving rise to the largest ratio (5.25) among the inks. It provides a balance between wettability, adhesion, cohesion, and debonding that leads to a relatively high tack. The combination possesses a lower G' than pristine CB028 at low frequency while also displaying a significantly higher (~3×) G' at high frequency. Thus, the synergistic effects of PO and EC that were observed in the viscoelastic recovery experiments are reinforced in the ratios presented in Table 2.

Tack and Peel Test. To further quantify and visualize the effects of the additives on CB028, tack and peel tests were also performed by using a rheometer. As presented in a previous section, the tack of viscoelastic ink is a complex property dependent on the synergy between adhesion and cohesion. It encompasses wettability, surface energy, contact time, application pressure, and bulk viscoelastic properties.[65,68] The ratios presented in Table 2 can be used to make general inferences; however, more intentional testing methods using a rheometer can yield both the tack and peel performance. Figure 3 presents the results of the tack experiments, where the normal stress is plotted as a function of plate separation. During the test, the ink sample is initially confined between the two parallel plates of the rheometer. The top plate is then raised at a constant rate, and the normal force is measured as a function of vertical separation. During the debonding stages of the tack test, air can penetrate the ink forming air pockets that propagate into fibrillar formations as the ink deforms and peels from the substrate.[69] Theory suggests a strong correlation between the debonding resistance of polymeric materials and the formation and deformation of fibrillar structures in the material as the rheometer plates separate.[70] The peak of the curve in Figure 3 quantifies the tack, while the area under the curve quantifies the peel strength.[64,71] The values of the tack and peel strength are given in Table 3. In the inset of Figure 3, illustrations display the four stages of separation that occur during this process. The experiment reveals the tensile debonding behavior that occurs at the peel front (adhesion properties) in addition to the cavitation behavior and

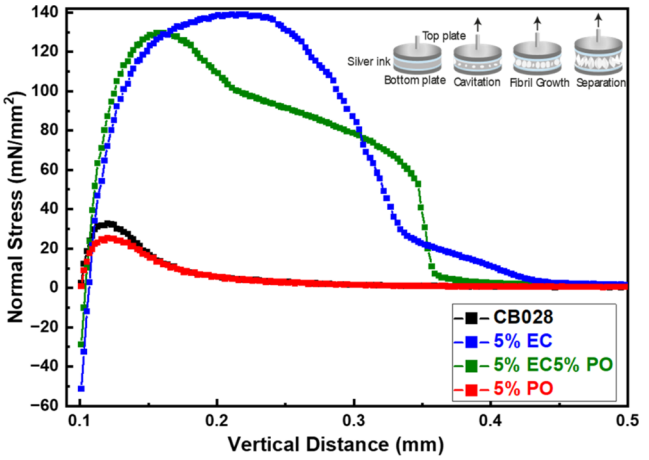

Figure 3. Normal stress as a function of the plate separation distance for the different formulations (tack test). The schematic in the figure represents the different stages of the test as the plates are pulled apart.

Table 3. Tack and Peel Strength of the Different Formulations as Calculated from Figure 3

ink	tack (mN/mm²)	peel resistance (kJ/mm²)
CB028	33	2.48
5%EC	140	26.92
5%EC5%PO	129	23.23
5%PO	25	1.12

deforming fibrillar structures that can rupture as the ink adheres to the substrate as the rheometer plates separate (cohesion properties).[64]

The results on the tack behavior reinforce the idea that the addition of EC and PO have contrasting effects on elasticity. EC facilitates high entanglement and network formation that restrict molecular motion and enhance the cohesive strength. As explained by molecular theory, high cohesive strength has been a prerequisite for high adhesion.[72] The formulations without EC displayed low tack compared to the formulations that contained EC. The addition of EC increased tack performance by 4-fold. As presented in Figure 3, pristine CB028, 5%EC, and 5%EC5%PO, 5%PO showed normal stress peaks of 33, 140, 130, and 25 mN/mm², respectively. Peel strength was also significantly enhanced by EC. When EC is combined with PO, the ink exhibited a higher peel strength (23.23 kJ/m²) than that of pristine CB028 (2.48 kJ/m²) and was comparable to that of 5%EC (26.92 kJ/m²). The results reinforce the calculated tack ratios in Table 2 from the frequency sweep experiments. Fibrillar structures were also more pronounced with the presence of EC because of high cohesion[70] and highlight its importance in improving the stickiness and tack of the ink as it forms an interface with the substrate. Figure S2, in the Supporting Information, presents

https://doi.org/10.1021/acsomega.4c09042
ACS Omega 2025, 10, 1429−1439

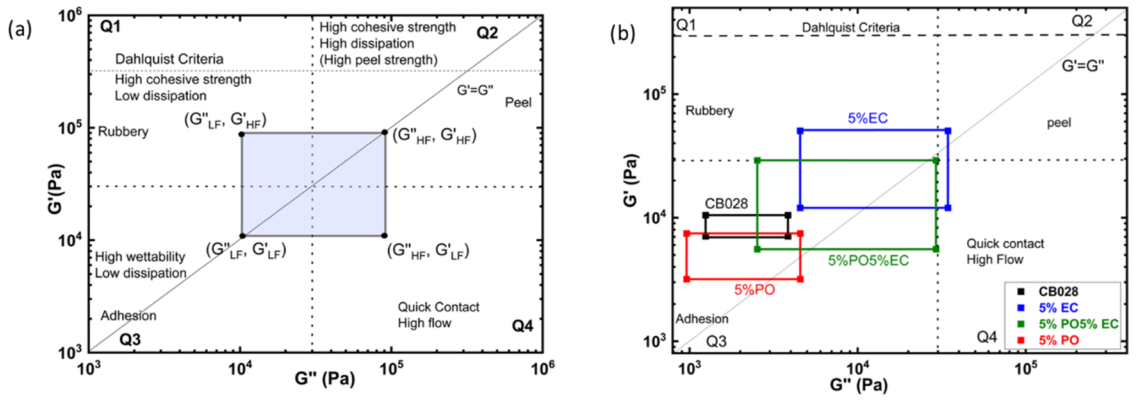

Figure 4. Viscoelastic window (VW) analysis: (a) Illustration of construction and analysis of VW for determining the adhesive and cohesive properties. (b) Constructed VW of the CB028 ink formulation. The addition of EC and PO influences the bonding and debonding behaviors of CB028.

photos of the fibrillar structures illustrated in the inset of Figure 3.

Viscoelastic Windows (VWs). Frequency sweep, G' ratio at high and low frequencies, and tack experiments have provided beneficial information about the bonding and debonding behaviors of viscoelastic inks. To formulate inks that possesses the combination of wettability, tack, and peel strength, guidelines for tuning can be established using a graphical technique proposed by Chang.[63] The moduli data at low (0.1 Hz) and high (10 Hz) frequencies can be plotted to construct viscoelastic windows (VWs) for each ink for visual comparisons. A sample VW is presented in Figure 4a, where LF and HF denote the low frequency and high-frequency moduli, respectively. The figure displays four quadrants based on moduli values: rubbery (Q1), high peel performance (Q2), high wettability (Q3), and high contact efficiency (Q4). The value of the storage modulus should be less than 3×10^5 Pa to ensure adequate adhesion according to the Dahlquist criteria.[73] This criterion is indicated in Figure 4a by a dotted line. In addition to the labeled Dahlquist threshold,[73] there exists diagonal crossover line that indicates the convergence of storage and loss modulus.[63] The left region of the line indicates elastic behavior ($G' > G''$), while the right portion indicates viscous behavior. To construct a window, G' and G'' serve as the y-coordinate and x-coordinate, respectively, and by plotting the experimental data according to the defined Cartesian coordinates, a rectangle can be constructed to represent the VW of each ink.

The loss moduli at both low frequency and high frequency establish the length of the VW. Longer bases, which imply higher values of the loss modulus (G'') at higher frequencies, are favorable for contact efficiency (more viscous at shorter time scales) and energy dissipation (higher loss modulus).[73] The storage moduli at low and high frequency establish the height of the VW with higher heights indicating increased peel strength.[63,65,74] The position of the base of the rectangle is an indicator of the wettability of the ink. Ideally, the additives used to formulate the ink should lower the position of the base for improved wettability, while also increasing the height of the rectangle. By increasing the height, the VW would maintain a position in Q2 signifying a high peel strength. Thus, an ideal VW has a long base, increased height, a lower position of the bottom-left vertex, and a higher position of the top-right vertex.

Figure 4b presents the VWs for the ink formulations developed in this work using the data in Table 2. The VW of CB028 (black rectangle) maintains both the lowest width and the lowest height and lies primarily in Q3. Thus, it exhibits both poor adhesion and peel strength and may break easily as a strain gauge. The addition of PO lowers the position of the VW (red), indicating improved wettability; however, the peel strength remains low. The addition of EC raises the position of the VW base (blue), representing reduced wettability; however, the increased rectangle height and position in Q2 indicate the highest peel strength among the ink formulations. As realized in Figure 2d and Table 2, the combination of EC and PO produced a VW (green) that has the longest base and height for all samples. Thus, this ink formulation displays a favorable balance of desired properties (wettability, cohesion, and peel strength) to form a robust ink/substrate interface that resists peeling during continuous strain operations. This will be explored further in the subsequent sections of this publication.

Inks Resistivity. The printed traces of each ink formulation were cured in an oven at 160 °C for one h before testing for resistivity. Several factors dictate resistivity, including the particle type, surface resistance, electron tunneling effects, and the polymer matrix.[42] The measured resistivity of CB028, 5% EC, 5%EC5%PO, and 5%PO were 9.94 ± 3.10, 31.82 ± 8.78, 94.10 ± 21.58, and 8.54 ± 1.88 $\mu\Omega$·cm, respectively. Figure 5 presents SEM images of the printed and cured formulations to establish structure−property relationships. Pristine CB028 maintains a lower resistivity; whereas, the addition of EC fills the gaps among the conductive particles with an insulating material, thus resulting in increased resistivity. On the contrary, adding PO induces the aggregation of conductive particles (as seen from Figure 5d), resulting in slightly decreased values of the resistivity. The combination of EC and PO fills the gaps among the particles, coats them, and also results in particle aggregation (Figure 5c). The effect of the additives coupled with reduction in silver wt % led to the highest electrical resistivity. That increased binder/polymer presence results in the enhanced adhesion, tack, and peel strength, as revealed in Table 2, Figures 3, and 4.

Sensing Performance. Strain gauge experiments were conducted to correlate the structural features and properties with the sensing performance. The experiments were performed in a three-point bending configuration to measure relative resistance change (and hence gauge the factor). Each sample was prestrained at 0.15%. Then, at a stroke rate of 3 mm/min, each sample was strained for up to 1.5% with the exception of 5%PO, which was strained up to 0.75%. At higher

https://doi.org/10.1021/acsomega.4c09042
ACS Omega 2025, 10, 1429−1439

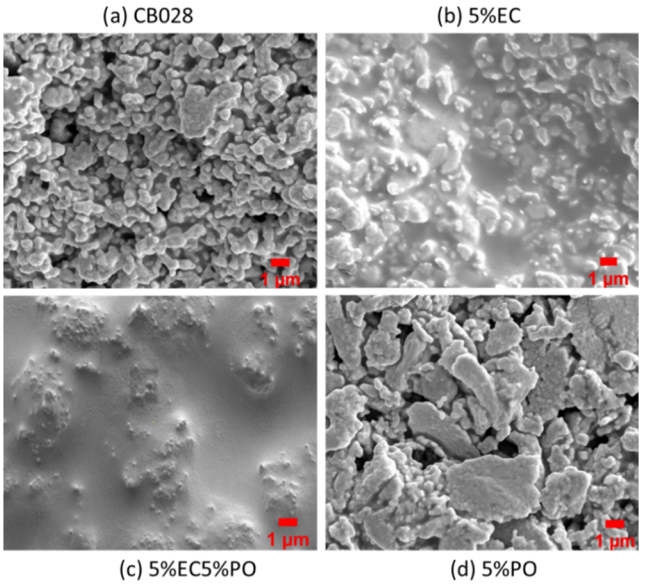

Figure 5. Scanning electron microscopy (SEM) images of formulated inks reveal the microstructure of the printed traces.

strains, the 5%PO samples peeled off of the PET substrate. The applied strain was sinusoidal and continued for 300 cycles. The relative resistance change for all samples is presented in Figure 6. CB028 has a high concentration (~70 wt %) of silver particles, which could make the trace brittle.[42,75] It exhibited a gauge factor as high as 11 (Figure 6a), which is relatively large compared to commercial metallic strain gauges (GF ~ 2).[8,76] However, the signal drift seen in Figure 6a can be attributed to the fewer binder traces displayed in the microscopy images in Figure 5a. Figure 7 presents microscopy images of the printed traces after strain cycles. The cracks developed in the traces printed from pristine CB028 (Figure 7a) reinforce the need for enhanced peel strength and flexibility. Addition of EC reduces the signal drift, as seen in the lower portion of the resistance response (Figure 6b). This is most likely due to the enhanced peel strength upon addition of EC as seen in previous sections. In the SEM image in Figure 7b, it is also apparent that 5%EC displayed enhanced flexibility by showing smaller and fewer microcracks in comparison to that of pristine CB028. The fewer cracks resulted in a response drift ($\Delta R/R_0$ at 1.5% strain) that subsided after ~130 cycles. The significant increase in gauge factor 208 (~20× more than CB028) may be due to the enhanced stress transfer facilitated by the polymer-filled interparticle spacings displayed in Figure 5b. Though the adhesion was improved, microcracks occurred, which can be attributed to the relative brittleness of EC upon curing. Mitigating that behavior would require the use of a plasticizer.[60,77]

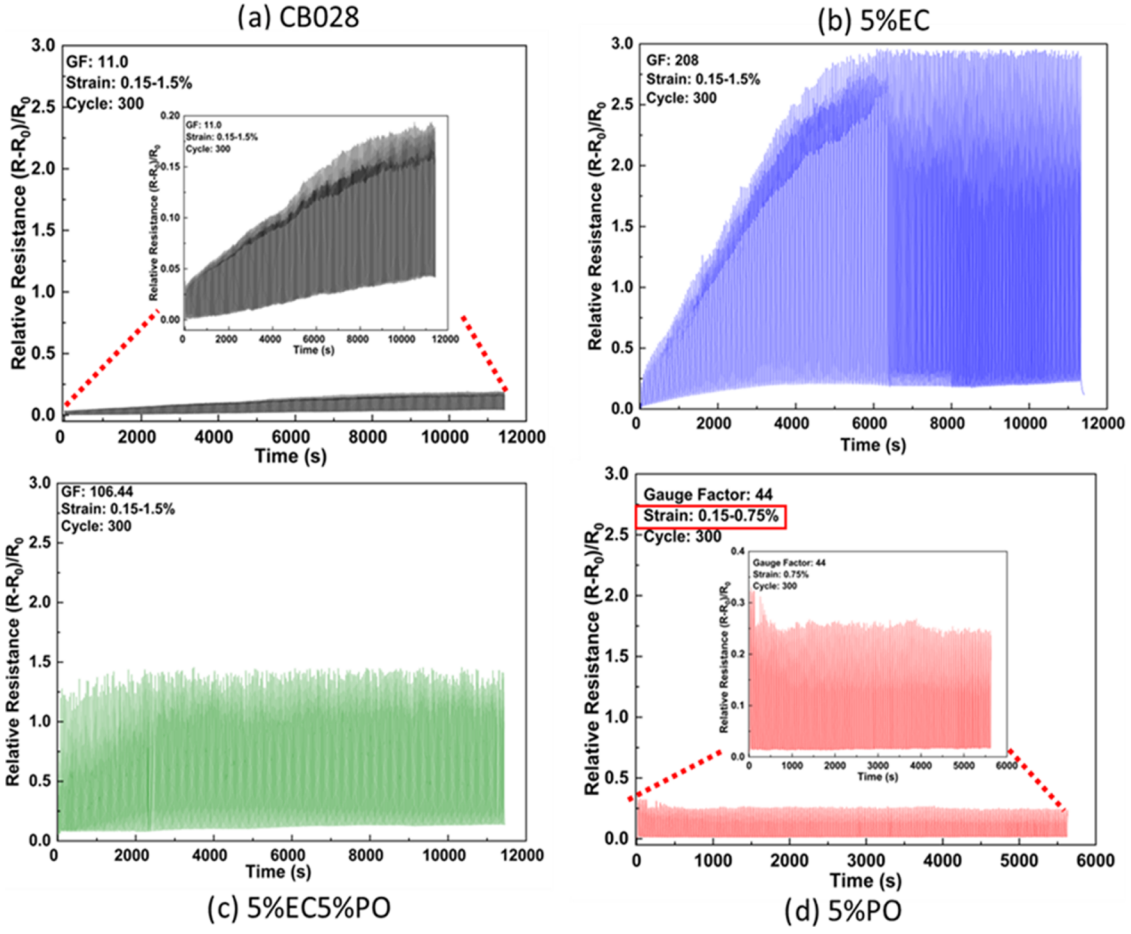

Figure 6. Performance tests of printed strain gauges using the CB028 ink formulations. Results reveal the long-term stability under repeated bending for 300 strain cycles (0.15−1.5%) for (a) pristine CB028, (b) 5%EC, and (c) 5%EC5%PO. Strain range was lowered to 0.15−0.75% for (d) 5%PO due to failures at higher strain percentages.

https://doi.org/10.1021/acsomega.4c09042
ACS Omega 2025, 10, 1429−1439

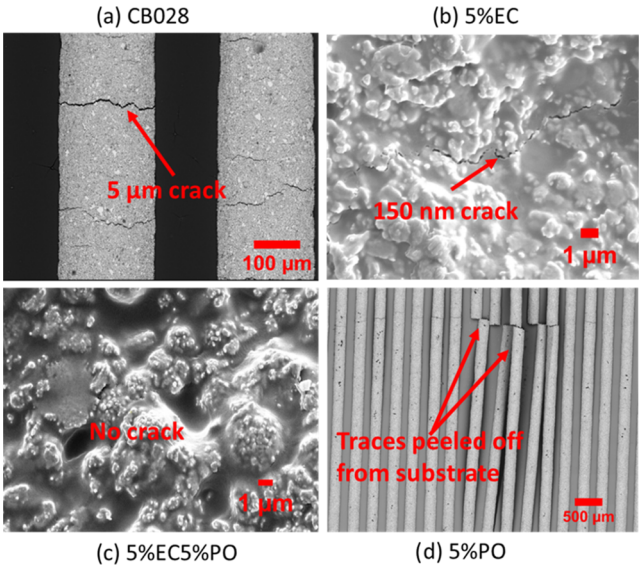

Figure 7. SEM images of ink formulations after sensing performance tests.

The 5%PO ink formulation exhibited a stable response but experienced poor flexibility due to the low cohesion and peel performance predicted in Table 2 and Figure 4b. The traces of 5%PO peeled off and broke at 1.5% strain, as presented in Figure 7d. In addition to being a diluent, PO serves as a plasticizer for the relatively brittle EC. PO occupies intermolecular spaces of the EC chain, preventing them from intercontact and, thereby, increasing the free volume. This increased free volume helps enhance the plasticity and flexibility of the EC-contained silver ink.[78] The 5%EC5%PO ink shows a gauge factor of 106 (Figure 6c) and significantly reduced crack formation due to the combined effect of EC and PO (Figure 7c). The two additives produced a balanced microstructure of coalesced particles and silver-polymer interactions that prevented both cracking and peeling off throughout the 300 cycles of bending strain, resulting in a stable and reliable sensing response. Though the gauge factor (~106) was not as high as 5%EC (~208), it was a magnitude higher than those of pristine CB028 (~11) and commercial strain gauges (~2).

CONCLUSIONS

This work formulated three inks from commercial CB028 (DuPont) silver ink by adding ethyl cellulose, polyolefin, and a combination of both polymers. The goal is to increase the gauge factor of the printed strain sensor while at the same time maintaining the flexibility of the traces. A systematic study of the rheological properties was coupled with 3D printing of the ink traces and subsequent testing of the flexibility and strain-sensing response. A viscoelastic window (VW) approach was developed based on the rheological data to determine if the inks exhibited the appropriate properties for reliable stain sensing. These properties included wettability, elasticity, and peel strength. Using the VW approach, it was realized that the combination of both EC and PO (90% CB028, 5% EC, and 5% PO) displayed synergy by improving the adhesion and cohesion. The tack value and peel strength for the formulated 5%EC5%PO were 129 mN/mm^2 and 23.23 kJ/m^2, respectively, significantly higher than commercial CB028. Microstructure studies revealed minimal cracks in the formulated ink after 300 cycles of bending strain. The flexibility of the ink resulted in the most stable response among the formulated inks while maintaining a gauge factor of 106, which is a magnitude higher than that of commercially available strain gauges. The developed rheology analysis coupled with the VW method thus holds promise for studying ink formulations for the DIW process. The resultant ink demonstrated good printing quality and significant gauge factor improvement, potentially for the on-demand production of sensitive and flexible strain gauges through direct ink writing.

ASSOCIATED CONTENT

Supporting Information

The Supporting Information is available free of charge at https://pubs.acs.org/doi/10.1021/acsomega.4c09042.

Schematic for measuring cross section of printed traces and fibrillar structures of inks formed during tack test (PDF)

AUTHOR INFORMATION

Corresponding Author

Subramanian Ramakrishnan − *Department of Chemical and Biomedical Engineering, FAMU-FSU College of Engineering, Tallahassee, Florida 32310, United States;* orcid.org/0000-0001-5108-2198; Email: srama@eng.famu.fsu.edu

Authors

Md Alamgir Hossain − *Department of Chemical and Biomedical Engineering, FAMU-FSU College of Engineering, Tallahassee, Florida 32310, United States*

Gabriela Plautz-Ratkovski − *Department of Chemical and Biomedical Engineering, FAMU-FSU College of Engineering, Tallahassee, Florida 32310, United States*

Joshua DeGraff − *High Performance Materials Institute, Department of Industrial and Manufacturing Engineering, Florida State University, Tallahassee, Florida 32310, United States*

Tarik J. Dickens − *High Performance Materials Institute, Department of Industrial and Manufacturing Engineering, Florida State University, Tallahassee, Florida 32310, United States*

Zhiyong Liang − *High Performance Materials Institute, Department of Industrial and Manufacturing Engineering, Florida State University, Tallahassee, Florida 32310, United States;* orcid.org/0000-0001-5099-9957

Curtis Hill − *Jacobs Space Exploration Group, NASA, Marshall Space Flight Center, Huntsville, Alabama 35812, United States*

Jennifer Jones − *NASA Marshall Space Flight Center, Huntsville, Alabama 35812, United States;* orcid.org/0000-0001-5655-1854

Complete contact information is available at: https://pubs.acs.org/10.1021/acsomega.4c09042

Notes

The authors declare no competing financial interest.

ACKNOWLEDGMENTS

We would like to acknowledge the funding from the National Aeronautics and Space Administration (NASA) under research of Cooperative Agreement Notice (CAN) under Grant Number ID#80MSFC21M0001. S.R. and Md.A.H. would

also like to acknowledge partial support from the NASA under Grant Number 80NSSC24K0416. G.P.-R. would like to acknowledge support from the NSF under Grant Number 2219558.

REFERENCES

(1) Wu, Q.; Okabe, Y.; Yu, F. Ultrasonic Structural Health Monitoring Using Fiber Bragg Grating. *Sensors* **2018**, *18* (10), 3395.
(2) Segev-Bar, M.; Haick, H. Flexible Sensors Based on Nanoparticles. *ACS Nano* **2013**, *7* (10), 8366−8378.
(3) Di Sante, R. Fibre Optic Sensors for Structural Health Monitoring of Aircraft Composite Structures: Recent Advances and Applications. *Sensors* **2015**, *15* (8), 18666−18713.
(4) Farrar, C. R.; Park, G.; Allen, D. W.; Todd, M. D. Sensor Network Paradigms for Structural Health Monitoring. *Struct. Control Health Monit.* **2006**, *13* (1), 210−225.
(5) Prosser, W. H.; Wu, M.-C.; Allison, S. G.; DeHaven, S. L.; Ghoshal, A. *Structural Health Monitoring Sensor Development at NASA Langley Research Center*; NASA Technical Report, Document ID: 20040085739, 2002.
(6) Güemes, A.; Fernandez-Lopez, A.; Pozo, A. R.; Sierra-Pérez, J. Structural Health Monitoring for Advanced Composite Structures: A Review. *J. Compos. Sci.* **2020**, *4* (1), 13.
(7) Abbas, S.; Li, F.; Qiu, J. A Review on SHM Techniques and Current Challenges for Characteristic Investigation of Damage in Composite Material Components of Aviation Industry. *Mater. Perform. Charact.* **2018**, *7* (1), 224−258.
(8) Amjadi, M.; Pichitpajongkit, A.; Lee, S.; Ryu, S.; Park, I. Highly Stretchable and Sensitive Strain Sensor Based on Silver Nanowire−Elastomer Nanocomposite. *ACS Nano* **2014**, *8* (5), 5154−5163.
(9) Amjadi, M.; Kyung, K.-U.; Park, I.; Sitti, M. Stretchable, Skin-Mountable, and Wearable Strain Sensors and Their Potential Applications: A Review. *Adv. Funct. Mater.* **2016**, *26* (11), 1678−1698.
(10) Xiao, X.; Yuan, L.; Zhong, J.; Ding, T.; Liu, Y.; Cai, Z.; Rong, Y.; Han, H.; Zhou, J.; Wang, Z. L. High-Strain Sensors Based on ZnO Nanowire/Polystyrene Hybridized Flexible Films. *Adv. Mater.* **2011**, *23* (45), 5440−5444.
(11) Lee, J.; Kim, S.; Lee, J.; Yang, D.; Park, B. C.; Ryu, S.; Park, I. A Stretchable Strain Sensor Based on a Metal Nanoparticle Thin Film for Human Motion Detection. *Nanoscale* **2014**, *6* (20), 11932−11939.
(12) Li, C.; Thostenson, E. T.; Chou, T.-W. Dominant Role of Tunneling Resistance in the Electrical Conductivity of Carbon Nanotube−Based Composites. *Appl. Phys. Lett.* **2007**, *91* (22), No. 223114, DOI: 10.1063/1.2819690.
(13) Neff, C.; Elston, E.; Burfeindt, M.; Crane, N.; Schrand, A. A Fundamental Study of Printed Ink Resiliency for Harsh Mechanical and Thermal Environmental Applications. *Addit. Manuf.* **2018**, *20*, 156−163.
(14) Liu, H.; Zhang, H.; Han, W.; Lin, H.; Li, R.; Zhu, J.; Huang, W. 3D Printed Flexible Strain Sensors: From Printing to Devices and Signals. *Adv. Mater.* **2021**, *33* (8), No. 2004782.
(15) Huang, P.; Xia, Z.; Cui, S. 3D Printing of Carbon Fiber-Filled Conductive Silicon Rubber. *Mater. Des.* **2018**, *142*, 11−21.
(16) Haney, R.; Tran, P.; Trigg, E. B.; Koerner, H.; Dickens, T.; Ramakrishnan, S. Printability and Performance of 3D Conductive Graphite Structures. *Addit. Manuf.* **2021**, *37*, No. 101618.
(17) Ibrahim, N.; Akindoyo, J. O.; Mariatti, M. Recent Development in Silver-Based Ink for Flexible Electronics. *J. Sci. Adv. Mater. Devices* **2022**, *7* (1), No. 100395.
(18) Lu, B.-H.; Lan, H.; Liu, H. Additive Manufacturing Frontier: 3D Printing Electronics. *Opto-Electron. Adv.* **2018**, *1* (1), No. 170004.
(19) Soe, H. M.; Manaf, A. A.; Matsuda, A.; Jaafar, M. Development and Fabrication of Highly Flexible, Stretchable, and Sensitive Strain Sensor for Long Durability Based on Silver Nanoparticles−Polydimethylsiloxane Composite. *J. Mater. Sci. Mater. Electron.* **2020**, *31*, 11897−11910.
(20) Qi, X.; Ha, H.; Hwang, B.; Lim, S. Printability of the Screen-Printed Strain Sensor with Carbon Black/Silver Paste for Sensitive Wearable Electronics. *Appl. Sci.* **2020**, *10* (19), 6983.
(21) Wang, Y.-F.; Sekine, T.; Takeda, Y.; Hong, J.; Yoshida, A.; Matsui, H.; Kumaki, D.; Nishikawa, T.; Shiba, T.; Sunaga, T.; Tokito, S. Printed Strain Sensor with High Sensitivity and Wide Working Range Using a Novel Brittle−Stretchable Conductive Network. *ACS Appl. Mater. Interfaces* **2020**, *12* (31), 35282−35290.
(22) Kim, S.-R.; Kim, J.-H.; Park, J.-W. Wearable and Transparent Capacitive Strain Sensor with High Sensitivity Based on Patterned Ag Nanowire Networks. *ACS Appl. Mater. Interfaces* **2017**, *9* (31), 26407−26416.
(23) Boland, C. S.; Khan, U.; Benameur, H.; Coleman, J. N. Surface Coatings of Silver Nanowires Lead to Effective, High Conductivity, High-Strain, Ultrathin Sensors. *Nanoscale* **2017**, *9* (46), 18507−18515.
(24) Meng, Q.; Liu, Z.; Han, S.; Xu, L.; Araby, S.; Cai, R.; Zhao, Y.; Lu, S.; Liu, T. A Facile Approach to Fabricate Highly Sensitive, Flexible Strain Sensor Based on Elastomeric/Graphene Platelet Composite Film. *J. Mater. Sci.* **2019**, *54* (15), 10856−10870.
(25) Lin, Y.; Dong, X.; Liu, S.; Chen, S.; Wei, Y.; Liu, L. Graphene−Elastomer Composites with Segregated Nanostructured Network for Liquid and Strain Sensing Application. *ACS Appl. Mater. Interfaces* **2016**, *8* (36), 24143−24151.
(26) Chen, J.; Zhu, Y.; Jiang, W. A Stretchable and Transparent Strain Sensor Based on Sandwich-like PDMS/CNTs/PDMS Composite Containing an Ultrathin Conductive CNT Layer. *Compos. Sci. Technol.* **2020**, *186*, No. 107938.
(27) Xiang, D.; Zhang, X.; Harkin-Jones, E.; Zhu, W.; Zhou, Z.; Shen, Y.; Li, Y.; Zhao, C.; Wang, P. Synergistic Effects of Hybrid Conductive Nanofillers on the Performance of 3D Printed Highly Elastic Strain Sensors. *Composites, Part A* **2020**, *129*, No. 105730.
(28) Zhao, S.; Guo, L.; Li, J.; Li, N.; Zhang, G.; Gao, Y.; Li, J.; Cao, D.; Wang, W.; Jin, Y.; et al. Binary Synergistic Sensitivity Strengthening of Bioinspired Hierarchical Architectures Based on Fragmentized Reduced Graphene Oxide Sponge and Silver Nanoparticles for Strain Sensors and Beyond. *Small* **2017**, *13* (28), No. 1700944.
(29) Li, Q.; Li, J.; Tran, D.; Luo, C.; Gao, Y.; Yu, C.; Xuan, F. Engineering of Carbon Nanotube/Polydimethylsiloxane Nanocomposites with Enhanced Sensitivity for Wearable Motion Sensors. *J. Mater. Chem. C* **2017**, *5* (42), 11092−11099.
(30) Gu, H.; Guo, J.; Wei, H.; Guo, S.; Liu, J.; Huang, Y.; Khan, M. A.; Wang, X.; Young, D. P.; Wei, S.; Guo, Z. Strengthened Magnetoresistive Epoxy Nanocomposite Papers Derived from Synergistic Nanomagnetite-Carbon Nanofiber Nanohybrids. *Adv. Mater.* **2015**, *27* (40), 6277−6282.
(31) Kim, S. Y.; Noh, Y. J.; Yu, J. Improved Thermal Conductivity of Polymeric Composites Fabricated by Solvent-Free Processing for the Enhanced Dispersion of Nanofillers and a Theoretical Approach for Composites Containing Multiple Heterogeneities and Geometrized Nanofillers. *Compos. Sci. Technol.* **2014**, *101*, 79−85.
(32) Peng, P.; Li, L.; Guo, W.; Hui, Z.; Fu, J.; Jin, C.; Liu, Y.; Zhu, Y. Room-Temperature Joining of Silver Nanoparticles Using Potassium Chloride Solution for Flexible Electrode Application. *J. Phys. Chem. C* **2018**, *122* (5), 2704−2711.
(33) Chen, S.; Guan, Y.; Li, Y.; Yan, X.; Ni, H.; Li, L. A Water-Based Silver Nanowire Ink for Large-Scale Flexible Transparent Conductive Films and Touch Screens. *J. Mater. Chem. C* **2017**, *5* (9), 2404−2414.
(34) Huang, H.-J.; Ning, X.; Zhou, M.-B.; Sun, T.; Wu, X.; Zhang, X.-P. A Three-Dimensional Printable Liquid Metal-like Ag Nanoparticle Ink for Making a Super-Stretchable and Highly Cyclic Durable Strain Sensor. *ACS Appl. Mater. Interfaces* **2021**, *13* (15), 18021−18032.
(35) Im, H.-G.; Jin, J.; Ko, J.-H.; Lee, J.; Lee, J.-Y.; Bae, B.-S. Flexible Transparent Conducting Composite Films Using a Monolithically Embedded AgNW Electrode with Robust Performance Stability. *Nanoscale* **2014**, *6* (2), 711−715.

(36) Kim, I.; Woo, K.; Zhong, Z.; Ko, P.; Jang, Y.; Jung, M.; Jo, J.; Kwon, S.; Lee, S.-H.; Lee, S.; et al. A Photonic Sintering Derived Ag Flake/Nanoparticle-Based Highly Sensitive Stretchable Strain Sensor for Human Motion Monitoring. *Nanoscale* **2018**, *10* (17), 7890−7897.
(37) Glatz-Reichenbach, J.; Glatz-Reichenbach, J. Feature Article Conducting Polymer Composites. *J. Electroceram.* **1999**, *3* (4), 329−346.
(38) Pekarovicova, A.; Husovska, V. Printing Ink Formulations. *Print. Polym.* **2016**, 41−55.
(39) Cano-Raya, C.; Denchev, Z. Z.; Cruz, S. F.; Viana, J. C. Chemistry of Solid Metal-Based Inks and Pastes for Printed Electronics−A Review. *Appl. Mater. Today* **2019**, *15*, 416−430.
(40) Rane, S. B.; Seth, T.; Phatak, G. J.; Amalnerkar, D. P.; Ghatpande, M. Effect of Inorganic Binders on the Properties of Silver Thick Films. *J. Mater. Sci. Mater. Electron.* **2004**, *15*, 103−106.
(41) Lai, C. Y.; Cheong, C. F.; Mandeep, J. S.; Abdullah, H. B.; Amin, N.; Lai, K. W. Synthesis and Characterization of Silver Nanoparticles and Silver Inks: Review on the Past and Recent Technology Roadmaps. *J. Mater. Eng. Perform.* **2014**, *23*, 3541−3550.
(42) Merilampi, S.; Laine-Ma, T.; Ruuskanen, P. The Characterization of Electrically Conductive Silver Ink Patterns on Flexible Substrates. *Microelectron. Reliab.* **2009**, *49* (7), 782−790.
(43) Fu, L. Laser Curing of Inks for Plastic Electronic Applications. PhD Thesis, University of Liverpool, 2014.
(44) Rogers, J. E. In *On the Bending Effects of a Printed 4 × 4 Antenna Array*, 2021 IEEE 21st Annual Wireless and Microwave Technology Conference (WAMICON); IEEE, 2021; pp 1−6.
(45) Sekine, T.; Fukuda, K.; Kumaki, D.; Tokito, S. Enhanced Adhesion Mechanisms between Printed Nano-Silver Electrodes and Underlying Polymer Layers. *Nanotechnology* **2015**, *26* (32), No. 321001.
(46) Soe, H. M.; Abd Manaf, A.; Matsuda, A.; Jaafar, M. Performance of a Silver Nanoparticles-Based Polydimethylsiloxane Composite Strain Sensor Produced Using Different Fabrication Methods. *Sens. Actuators, A* **2021**, *329*, No. 112793.
(47) Li, Y.; Chen, Y.; Yang, Y.; Gu, J.-D.; Ke, K.; Yin, B.; Yang, M.-B. Aligned Wave-like Elastomer Fibers with Robust Conductive Layers via Electroless Deposition for Stretchable Electrode Applications. *J. Mater. Chem. B* **2021**, *9* (42), 8801−8808.
(48) Heng, P. W. S.; Chan, L. W.; Chow, K. T. Development of Novel Nonaqueous Ethylcellulose Gel Matrices: Rheological and Mechanical Characterization. *Pharm. Res.* **2005**, *22* (4), 676−684.
(49) Davidovich-Pinhas, M.; Barbut, S.; Marangoni, A. G. Physical Structure and Thermal Behavior of Ethylcellulose. *Cellulose* **2014**, *21* (5), 3243−3255.
(50) Rekhi, G. S.; Jambhekar, S. S. Ethylcellulose-a Polymer Review. *Drug Dev. Ind. Pharm.* **1995**, *21* (1), 61−77.
(51) Fang, Q.; Lafdi, K. Effect of Nanofiller Morphology on the Electrical Conductivity of Polymer Nanocomposites. *Nano Express* **2021**, *2* (1), No. 010019.
(52) Wilson, S. A.; Cross, L. M.; Peak, C. W.; Gaharwar, A. K. Shear-Thinning and Thermo-Reversible Nanoengineered Inks for 3D Bioprinting. *ACS Appl. Mater. Interfaces* **2017**, *9* (50), 43449−43458.
(53) Liu, Z.; Bhandari, B.; Prakash, S.; Mantihal, S.; Zhang, M. Linking Rheology and Printability of a Multicomponent Gel System of Carrageenan-Xanthan-Starch in Extrusion Based Additive Manufacturing. *Food Hydrocolloids* **2019**, *87*, 413−424.
(54) Son, Y. Determination of Shear Viscosity and Shear Rate from Pressure Drop and Flow Rate Relationship in a Rectangular Channel. *Polymer* **2007**, *48* (2), 632−637.
(55) Kerminen, J.; Wiklund, J.; Karakoç, A.; Ruttik, K.; Jäntti, R.; Yiğitler, H. Characterization of Low-Cost Inkjet Printed-Photonic Cured Strain Gauges for Remote Sensing and Structural Monitoring Applications. *Res. Eng. Struct. Mater.* **2021**, *7*, 647−660, DOI: 10.17515/resm2021.360me1029.
(56) Kang, H.; Kim, S.; Shin, J.; Ko, S. Inkjet-Printed Flexible Strain-Gauge Sensor on Polymer Substrate: Topographical Analysis of Sensitivity. *Appl. Sci.* **2022**, *12* (6), 3193.
(57) ASTM D 257-14: Standard Test Method for DC Resistance of Conductance of Insulating Materials.
(58) ASTM D7264/D7264M-07: Standard Test Method for Flexural Properties of Polymer Matrix Composite Materials.
(59) Sweeney, M.; Campbell, L. L.; Hanson, J.; Pantoya, M. L.; Christopher, G. F. Characterizing the Feasibility of Processing Wet Granular Materials to Improve Rheology for 3D Printing. *J. Mater. Sci.* **2017**, *52*, 13040−13053.
(60) Vieira, M. G. A.; Da Silva, M. A.; Dos Santos, L. O.; Beppu, M. M. Natural-Based Plasticizers and Biopolymer Films: A Review. *Eur. Polym. J.* **2011**, *47* (3), 254−263.
(61) Feldstein, M. M.; Dormidontova, E. E.; Khokhlov, A. R. Pressure Sensitive Adhesives Based on Interpolymer Complexes. *Prog. Polym. Sci.* **2015**, *42*, 79−153.
(62) Jackson, S.; Dickens, T. Rheological and Structural Characterization of 3D-Printable Polymer Electrolyte Inks. *Polym. Test.* **2021**, *104*, No. 107377.
(63) Chang, E. P. Viscoelastic Properties of Pressure-Sensitive Adhesives. *J. Adhes.* **1997**, *60* (1−4), 233−248.
(64) Da Silva, L. F.; Öchsner, A.; Adams, R. D. *Handbook of Adhesion Technology*; Springer Science & Business Media, 2011.
(65) Fuensanta, M.; Vallino-Moyano, M. A.; Martín-Martínez, J. M. Balanced Viscoelastic Properties of Pressure Sensitive Adhesives Made with Thermoplastic Polyurethanes Blends. *Polymers* **2019**, *11* (10), 1608.
(66) Whitten, P. G.; Brown, H. R. Polymer Entanglement Density and Its Influence on Interfacial Friction. *Phys. Rev. E* **2007**, *76* (2), No. 026101.
(67) Mazzeo, F. A. *Characterization of Pressure Sensitive Adhesives by Rheology*; TA Instruments Report RH082, 2002; pp 1−8.
(68) Tordjeman, P.; Papon, E.; Villenave, J.-J. Tack Properties of Pressure-Sensitive Adhesives. *J. Polym. Sci., Part B: Polym. Phys.* **2000**, *38* (9), 1201−1208.
(69) Lakrout, H.; Sergot, P.; Creton, C. Direct Observation of Cavitation and Fibrillation in a Probe Tack Experiment on Model Acrylic Pressure-Sensitive-Adhesives. *J. Adhes.* **1999**, *69* (3−4), 307−359.
(70) Zosel, A. The Effect of Fibrilation on the Tack of Pressure Sensitive Adhesives. *Int. J. Adhes. Adhes.* **1998**, *18* (4), 265−271.
(71) Creton, C.; Hu, G.; Deplace, F.; Morgret, L.; Shull, K. R. Large-Strain Mechanical Behavior of Model Block Copolymer Adhesives. *Macromolecules* **2009**, *42* (20), 7605−7615.
(72) Feldstein, M. M.; Siegel, R. A. Molecular and Nanoscale Factors Governing Pressure-Sensitive Adhesion Strength of Viscoelastic Polymers. *J. Polym. Sci., Part B: Polym. Phys.* **2012**, *50* (11), 739−772.
(73) Dahlquist, C. A. Pressure-Sensitive Adhesives. *Treatise Adhes. Adhes.* **1969**, *2*, 219−260.
(74) Dillard, D. A.; Pocius, A. V.; Chaudhury, M. *Adhesion Science and Engineering*; Elsevier, 2002; Vol. *1*.
(75) Kirikova, M. N.; Agina, E. V.; Bessonov, A. A.; Sizov, A. S.; Borshchev, O. V.; Trul, A. A.; Muzafarov, A. M.; Ponomarenko, S. A. Direct-Write Printing of Reactive Oligomeric Alkoxysilanes as an Affordable and Highly Efficient Route for Promoting Local Adhesion of Silver Inks on Polymer Substrates. *J. Mater. Chem. C* **2016**, *4* (11), 2211−2218.
(76) Cao, H.; Thakar, S. K.; Oseng, M. L.; Nguyen, C. M.; Jebali, C.; Kouki, A. B.; Chiao, J.-C. Development and Characterization of a Novel Interdigitated Capacitive Strain Sensor for Structural Health Monitoring. *IEEE Sens. J.* **2015**, *15* (11), 6542−6548.
(77) Liu, J.; Guo, Q.; Mao, S.; Chen, Z.; Zhang, X.; Yang, Y.; Zhang, X. Templated Synthesis of a 1D Ag Nanohybrid in the Solid State and Its Organized Network for Strain-Sensing Applications. *J. Mater. Chem. C* **2018**, *6* (40), 10730−10738.
(78) Karger-Kocsis, J. *Polypropylene Structure, Blends and Composites: Vol. 3 Composites*; Springer Science & Business Media, 2012.

https://doi.org/10.1021/acsomega.4c09042
ACS Omega 2025, 10, 1429−1439